Potential risks of soil erosion in North-Central Vietnam using remote sensing and GIS[1]

Riscos potenciais de erosão do solo no centro-norte do Vietnã usando sensoriamento remoto e GIS

Nguyen T. T. Ha[2,3], Tran T. Tuyen[2], Astarkhanova T. Sarzhanovna[3], Hoang T. Thuy[2], Vu V. Luong[2], Tran D. Du[2], Dau K. Tai[2], Hoang A. The[2], Nguyen N. Thanh[2,4], Phung T. Duong[5]*, Vo T. T. Ha[2] & Vo T. N. Khanh[2,6]

[1] Research developed at Vinh University, Nghe An, Vietnam
[2] Vinh University, Nghe An, Vietnam
[3] Patrice Lumumba Peoples' Friendship University of Russia, Russia
[4] Novosibirsk State Agrarian University, Russia
[5] Dong Thap University, Vietnam
[6] Vinh University/High School for the Gifted Students, Nghe An, Vietnam

HIGHLIGHTS:

Soil erosion increased under the accelerating frequency of extreme rainfall events.
Applying suitable approach methods contributes to enhancing the predictability of the land cover change (LCC).
The decline in the vegetation covers caused an increasing trend in the soil erosion.

ABSTRACT: Unsustainable exploitation activities (UEAs), combined with the increasing impacts of global climate change are the key causes that lead to soil erosion in the North-Central Vietnam. Mountainous areas in the North-Central Vietnam commonly have steep slopes and sandy clay in the surface soil layer, which contribute to enhancing the soil erosion, resulting in a serious loss of life and property. This study investigates the land cover change (LCC) across the Thanh Chuong district by combining Remote Sensing Technique (RST) data with Geographic Information System (GIS) and further, establishing erosion risk hazard maps based on the RUSLE model simulation. To achieve these objectives, Sentinel and Landsat satellite images from the period 2010_2021 were acquired. It was verified that the forest area gradually decreased from 2010_2021, and the average annual soil loss was approximately 25 t per year. The amount of erosion that led to a soil loss of up to 18% of the total land area is related to weather conditions, terrain features, and the soil texture. The decline in the vegetation cover is expected to be the main cause of increasing trends in erosion and soil loss.

Key words: erosion risk map, ecosystem service, soil erosion, sentinel, RUSLE

RESUMO: Atividades de exploração insustentáveis (UEAs), combinadas com os crescentes impactos das mudanças climáticas globais são as principais causas que levam à erosão do solo no centro-norte do Vietnã. As áreas montanhosas no centro-norte do Vietnã geralmente têm encostas íngremes e argila arenosa na camada superficial do solo, o que contribui para aumentar a erosão do solo, resultando em uma séria perda de vidas e propriedades. Este estudo investiga a mudança de cobertura da terra (LCC) em todo o distrito de Thanh Chuong combinando dados da técnica de sensoriamento remoto (RST) com o Sistema de Informação Geográfica (GIS) e, além disso, estabelecendo mapas de risco de erosão com base na simulação do modelo RUSLE. Para atingir estes objetivos, foram adquiridas imagens dos satélites Sentinel e Landsat do período 2010-2021. Verificou-se que a área florestal diminuiu gradualmente de 2010-2021, e a perda média anual de solo foi de aproximadamente 25 t por ano. A quantidade de erosão que levou a uma perda de solo de até 18% da área total da terra está relacionada às condições climáticas, características do terreno e textura do solo. Espera-se que o declínio da cobertura vegetal seja a principal causa das tendências crescentes de erosão e perda de solo.

Palavras-chave: mapa de risco de erosão, mudança de cobertura da terra, erosão do solo, sentinela, RUSLE

INTRODUCTION

Soil loss due to erosion has serious environmental consequences (Abdo & Salloum, 2017; Vijith & Dodge, 2017) that are considered natural disasters (Allafta & Opp, 2022; Amellah & El-Morabiti, 2021). Soil erosion is accelerated by human activities, and the impacts of climate change have become a global problem (Brodie & Catherine, 2020; Dang, 2021). Studies on soil erosion for implementation of land use and management practices (LUMPs) are considered one of the key components needed to provide early warnings to minimise the damage to people and property caused by erosion (Mohamed et al., 2020). According to Brodie & Catherine (2020), soil erosion commonly depends on factors such as weather conditions, the shape of the watershed, the soil texture, and land use management practices. Studies on soil erosion, therefore, are difficult to carry out because of the complex relationships among the governing factors (Lin & Peng, 2022; Yesuph & Dagnew, 2019).

Today, with the advent of remote sensing techniques (RSTs), a combination of geographic information system (GIS) and RST data has been found to be an efficient support tool for studying the the land cover change (LCC) (Khwarahm et al., 2021; Sapkale et al., 2022). Due to the superiority of the combination of GIS and RST data with erosion models, numerous studies on the LCC have been widely employed around the world (Allafta & Opp, 2022; Khwarahm et al., 2021). Instance typical studies of Gitas et al. (2009) in Greece, Khwarahm et al. (2021) in Iraq, and Allafta & Opp (2022) in the Shatt Al-Arab basin of Iraq-Iran.

In recent years, the North-Central Vietnam has regularly suffered from soil erosion due to the increased number of extreme weather events. Unsustainable exploitation activities (UEAs) are contributing to this increase in soil erosion (Fachin et al., 2021; Sapkale et al., 2022). The main objective of this study investigates the LCC across the Thanh Chuong Mountainous district of Nghe An province based on a combination of GIS and RST and the RUSLE model.

MATERIALS AND METHODS

The study area is located southwest of Nghe An province, (18° 34' 42" N-18° 53' 33" N and 104° 56' 07" E-05° 36' 06" E), and it covers an area of 1228 km² with a population of approximately 250,000 people (Dinh & Kazuto, 2022; Do, 2020). The topography of the area is very diverse, with the main forms of topography being the mountains and midlands; the altitude ranges from less than 10 m a.m.s.l to more than 1500 m a.m.s.l (Figure 1). It is gradually tilted from north to south and from west to east (Dinh & Kazuto, 2022; Hung et al., 2017).

Thanh Chuong is known as a centre of agricultural and forestry production, and the income of local people depends on products obtained from agricultural production, harvesting timber, and ecosystem service (Dinh & Kazuto, 2022; Do, 2020). Mountainous regions are threatened by high rates of soil loss due to erosion, leading to soil degradation (Do, 2020; Hung et al., 2017). In addition, UEAs have contributed to exposing bare soil areas without vegetation cover, causing the

Figure 1. The topographic map of the study area

potential risks for soil erosion (Amellah & El-Morabiti, 2021; Dinh & Kazuto, 2022).

Natural disasters such as extreme rainfall events, cyclone, tropical storms have appeared frequently during the rainy season period (May to November), causing flash floods result in soil erosion (Tue et al., 2015; Dinh & Kazuto, 2022). To achieve the objectives of this study, maps of the spatial-temporal distribution of the land use were obtained from Landsat (https://glovis.usgs.gov), and Sentinel images (https://scihub.copernicus.eu). Sets of images with a resolution of 30 m were taken from 2010_2021 (Table 1). Before the remote sensing image classification process, the downloaded images were processed using the ENVI software (Version 4.7). To obtain a high-precision image covering the entire study area, the atmospheric correction was conducted so that the vegetation spectrum curve obtained was close to the real vegetation spectrum. In addition, the image processing procedures are also conducted including radiometric, atmospheric, geometric, and topographic corrections.

In order to decrease the differences between the Landsat and remote sensing images, the digital elevation model (DEM) dataset was resampled based on the grid snap technique; all of the resampled images lined up exactly. In addition, to enhance the quality of the images, pre-processing steps were applied to the satellite images, including the conversion of the digital numerical values of the image to the top_of_atmosphere reflectance using atmospheric correction and the resampling of the resolution from 30 to 10 m; atmospheric correction of Sentinel- 2A images was conducted by applying a semi-automatic classification process based on a plugin tool in the QGIS software (Version 3.16).

The RUSLE-Revised Universal Soil Loss Equation is a modification of the USLE-Universal Soil Loss Equation model that was developed by Wischmeier & Smith (1978). The model is widely applied for simulating surface soil loss in other areas around the world (Amellah & El-Morabiti; El-Jazouli et al., 2017). In the RUSLE model, changes in LUMPs are directly added as the input data which is contributed to its increased accuracy compared to the other soil erosion models (El-Jazouli et al., 2017). An advantage of the RUSLE model is that it easily collected input data through the conversion from DEM data to satellite images (El-Jazouli et al., 2017). The RUSLE model is

Table 1. Data concerning the satellite images used in this study

Data	Projection	Acquisition data	Resolution (m)	Source
Landsat 5 TM	UTM-Zone-48N	2000	30	https://glovis.usgs.gov/
Landsat 5 TM	UTM-Zone-48N	2001	30	
Landsat 5 TM	UTM-Zone-48N	2002	30	
Landsat 5 TM	UTM-Zone-48N	2003	30	
Landsat 5 TM	UTM-Zone-48N	2004	30	
Landsat 5 TM	UTM-Zone-48N	2005	30	
Landsat 5 TM	UTM-Zone-48N	2006	30	
Landsat 5 TM	UTM-Zone-48N	2007	30	
Landsat 5 TM	UTM-Zone-48N	2008	30	
Landsat 5 TM	UTM-Zone-48N	2009	30	
Landsat 5 TM	UTM-Zone-48N	2010	30	
Landsat 5 TM	UTM-Zone-48N	2011	30	
Landsat 5 TM	UTM-Zone-48N	2012	30	
Landsat 8 OLI	UTM-Zone-48N	2013	30	
Landsat 8 OLI	UTM-Zone-48N	2014	30	
Landsat 8 OLI	UTM-Zone-48N	2015	30	
Sentinel 2A	UTM-Zone-48N	2016	10	https://scihub.copernicus.eu/
Sentinel 2A	UTM-Zone-48N	2017	10	
Sentinel 2A	UTM-Zone-48N	2018	10	
Sentinel 2A	UTM-Zone-48N	2019	10	
Sentinel 2A	UTM-Zone-48N	2020	10	
Sentinel 2A	UTM-Zone-48N	2021	10	

constructed based on the integration of the five factors such as rainfall aggressivity, soil erodibility, inclination, slope length, land use, and anti-erosion practices.

The RUSLE model defines average annual soil loss through Eq. 1.

$$A = R \times K \times LS \times C \times P$$

where:

A - average annual spatial-temporal distribution of soil loss (t ha^{-1});

R - annual rainfall-runoff erosivity factor (MJ mm ha^{-1} h^{-1});

K - soil erodibility factor (Mg h MJ^{-1} mm^{-1});

LS - combination of the slope length and steepness factors, dimensionless;

C - cover and management factors, dimensionless; and,

P - support practices factor dimensionless.

The R_factor is commonly assumed as a function of rainfall's ability to cause soil erosion by dissecting and moving particles (Allafta & Opp, 2022). However, determining the R_factor is facing challenges due to the scarcity of high-resolution rainfall data.

The R_factor is, therefore, defined by Eq. 2.

$$R = 79 + 0.363 \times X_a$$

where:

Xa - the mean annual rainfall (mm).

The K_factor is considered as the reflection of the soil loss rate per runoff erosivity index due to rainfall. It was commonly evaluated based on the soil texture, organic matter, soil structure, and permeability (Abdo & Salloum, 2017). The K_factor is defined by Eq. 3.

$$K = 27.66 \times 10^{1.14} \times 10^{-8} \times (12 - a) +$$
$$+ 0.0043 \times (b - 2) + 0.0033 \times (c - 3)$$

where:

a - organic matter (%);

b - soil texture; and,

c - soil profile permeability.

While the LS_factor in Eq. 1 is computed by Eq. 4:

$$LS = \left[\frac{QaM}{22.13} \right] \times \left(0.065 + 0.045 \times S_g + 0.0065 \times S_g^2 \right)$$

where:

Qa - flow accumulation grid;

M - grid space size;

S$_g$ - grid slope in percentage; and,

y - dimensionless exponent that assumes the value varying from 0.2 to 0.5.

The C_factor is known as the cover and management factors which are dependent on vegetation type, stage of growth and coverage ability (El-Jazouli et al., 2017). The C_factor is obtained from reference tables (Ganasri & Ramesh, 2016) that are based on a range for known LUMP. Reference values of C_factor for the classes of LUMP applied in this work are presented in Table 2.

The P_factor in Eq. 1 is based on consideration of the influence of conservation solutions for each specific study area and is defined by Eq. 5.

$$P = 0.2 + 0.03 \times S$$

where:

S - the slope grade (%).

Table 2. The C_factor for different land use and management practices applied in the study

Class	C factor range	Mean value
Primary forest	0.001-0.002	0.0015
Plantation forest	0.01-0.02	0.015
Perennial plant	0.1-0.3	0.2
Annual plants	0.3-1.0	0.65
Other land	0.5-1.0	0.75
Waterbody	0	0

The overall methodology used in the present study is schematically represented in Figure 2.

The RUSLE model operates based on the integration of the five factors including rainfall, soil erodibility, topographic, cover and conservation practices, and support factor (Amellah & El-Morabiti; El-Jazouli et al., 2017). First, to run the model simulation, monthly rainfall data series from definning rainfall factors at six observation stations within the study area during the period of 2010_2021 were collected from the National Center for Hydro-Meteorological Forecasting, Vietnam. Distribution maps of R_factor across the study area are, then, obtained by transforming the observed rainfall series to the raster layers through applying Kriging interpolation method which integrated in the ArcGIS software (Figure 3A).
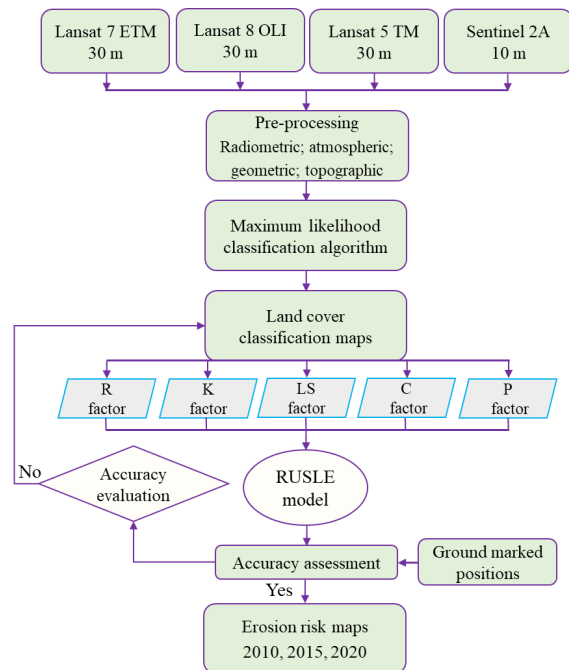
R-annual rainfall-runoff erosivity factor, K-soil erodibility factor, LS-the combination of the slope length and steepness factors, C-cover and management factors, P-support practices factor, and RUSLE-revised universal soil loss equation

Figure 2. Flowchart of the image processing procedures used to create an erosion risk map
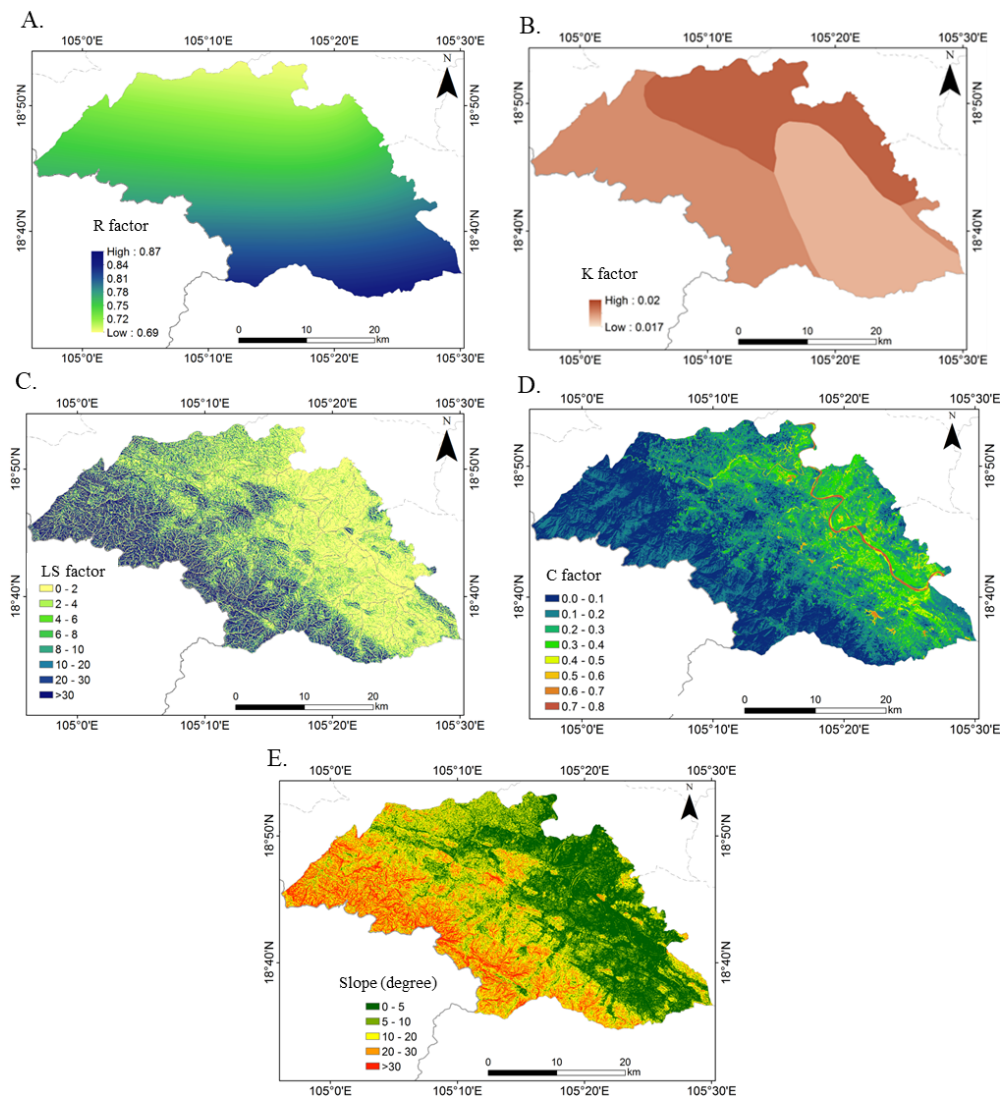
Figure 3. Distributions of (A) the R_factor, (B) the K_factor, (C) the LS_factor, (D) the C_factor and (E) the P_factor

Results and Discussion

According to Leh et al. (2013), the soil erosion rate in the mountainous areas with steep slopes is more sensitive to rainfall. The distribution map of the K_factor was defined based on the physicochemical properties of the soil which were collected through field surveys and then the soil texture was classified into six categories. The distribution map of the values of the K_factor was presented in Figure 3B. The topographic factor commonly represents the influence of the slope length and slope steepness on the erosion process, which is directly proportional to the slope's length and gradient (Khwarahm et al., 2021). Accordingly, the LS_factor was defined by considering the flow accumulation and slope (as percentages) as input (Leh et al. 2013). The LS_factor map was generated by using the DEM in the ArcGIS software and was presented in Figure 3C.

Based on research objectives, the area was classified into different six_cover classes, and the values of the C_factor were, therefore, derived from the area's land cover map that responds to land cover classes by conversing the raster map to vector format based on a supervised classification approach. The C_factor map was produced based on the LUMPs using spatial analysis tools as presented in Figure 3D. The P_factor represents the ratio of the soil loss, which is defined based on the control practices. Accordingly, for areas with good soil conservation solutions, the P_value is commonly taken because they limit runoff volume and velocity and promote sediment deposition on the slope surface. The soil erosion potential due to the runoff from rainfall events and their influence on basin features is expressed using the runoff on the surface soil (Figure 3E).

The accuracy of the land cover classification maps across the study area was quantified using ground-referenced data. The classification accuracy assessment was conducted for each land cover map, and it consisted of marking primary forest, plantation forest, perennial plants, annual plants, other plants, and water bodies using the field chips to verify the positions of ground_marked points using the GPS. The overall classification accuracies estimated for the Landsat images were 93 and 88%, respectively, while the Sentinel images had an estimated classification accurracy of 84%.

In addition, a comparison of the LCC maps for the years 2010, 2015, and 2021 developed using the RUSLE model and ground_marked real points was conducted based on statistical error indexes. An overall accuracy exceeding 90% confirmed that there was a good agreement between the simulated model and the observed data. This validation demonstrated the effectiveness of the applied model for simulating soil loss across the study area.

The land cover maps across the study area for 2010, 2015, and 2021 were classified into six classes (Figure 4A, B, C). In 2010, primary forest occupied the greatest area (up to 37200.2 ha), followed by other types of land (32832.0 ha), and plantation forest had the third_greatest area (around 23223.8 ha); meanwhile, the annual plant area was 12002.5 ha (10.70%), the perennial plant area was 5659.9 ha, and the water body area was only 1247.5 ha (Figure 4A, Table 3).

In general, the land cover changes mainly consist of primary and plantation forests with a total area of up to 60424.0 ha. The main reason that natural and plantation forests occupy the greatest area is that the forests are well protected, and agricultural expansion and infrastructure construction activities were not widely implemented during this period.

In 2015, there were 35117.4 ha of primary forest, 33554.5 ha of other land areas, 20233.3 ha of plantation forest, 17881.2 ha of annual plants, 4006.2 ha of perennial plants, and 1377.9 ha of water bodies (Figure 4). From 2010_2015, there were major declines in the primary forest coverage (2082.8 ha), plantation forest coverage (2990.5 ha), and perennial plant coverage (1653.7 ha), while the annual plant, other land, and water body areas showed slightly increasing trends (increasing by 5878.2, 722.5, and 130.4 ha, respectively).

The decline in the forest area and the increase in the plant land area may be due to agricultural expansion to serve the growing food needs of the local population. A study on the
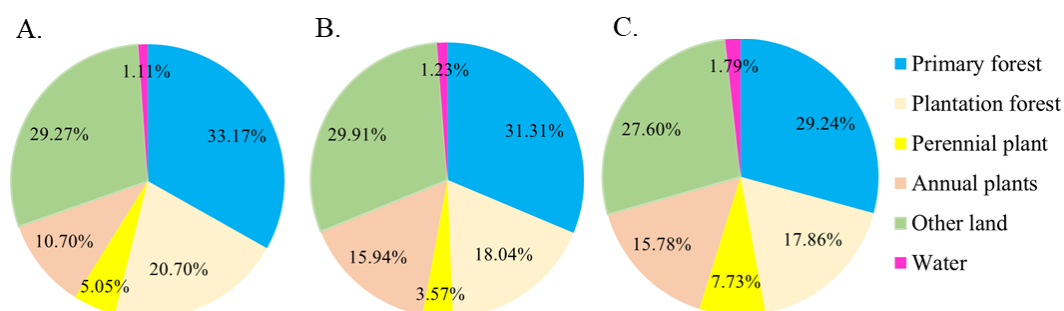

Figure 4. Land cover distribution in (A) 2010, (B) 2015, and (C) 2021

Table 3. The land cover change during the period from 2010-2021

Cover types	Total cover area (ha)			Changed trends in periods (%)		
	2010	2015	2021	2010-2015	2015-2021	2010-2021
Primary forest	37200.2	35117.4	32797.0	-1.86	-2.07	-3.92
Plantation forest	23223.8	20233.3	20027.3	-2.67	-0.18	-2.85
Perennial plant	5659.9	4006.2	8667.6	-1.47	+4.16	+2.68
Annual plants	12002.5	17881.2	17702.9	+5.24	-0.16	+5.08
Other land	32832.0	33554.5	30951.5	+0.64	-2.32	-1.67
Water	1247.5	1377.9	2012.1	+0.12	+0.57	+0.68

impacts of forest reclamation activities on soil properties by Dinh & Kazuto (2022) revealed that forests were exploited to serve the cultivation of acacia and cassava fields.

In 2021, primary and plantation forests experienced a sharp decline of 7599.7 ha, followed by other types of land, which decreased by 1880.5 ha. Conversely, the greatest expansion of the perennial and annual plant area of up to 8708.1 ha occurred during this time period, and a slightly increasing trend was also recorded for water bodies, which increased in area by approximately 764.6 ha. In general, primary and plantation forest areas continuously decreased from 2010_2021, while the cultivated soil areas continuously expanded. These results imply that the forest land area declined due to increasing pressure to expand agricultural activities. These findings indicate that the study area is facing the existential risks of land degradation, as well as an ecological environmental imbalance.

An erosion risk hazard map across the study area is presented in Figure 5. The results indicated that the soil loss due to erosion varied from 0_50 t ha^{-1} per year during the period from 2010_2021. The mean soil loss of 25 t ha^{-1} per year estimated by the RUSLE model simulation agrees with the observations. Figure 5 indicates that a few parts of the study area recorded a high soil loss, which may be due to steep slopes and the high intensity of rainfall events. It is observed that most parts of the study area experienced a low erosion level, which could be observed in almost all regions, while a high erosion level occurs only in a few regions where steep slopes with barren land exist due to UEAs. Moderate erosion is recorded from north_west to south_west in the study area where UEAs and steep slopes occur. The areas that showed an increase in the soil erosion are mainly located in the south_west and north_east parts of the study area because these regions are characterised by steep slopes and a hich rainfall intensity, while the east, south_east, and north_west parts of the study area experenced moderate soil erosion because they are characterised by gentle slopes and a lower rainfall intensity. Slight soil erosion is widely distributed throughout the study area.

These results could be interpreted as being due to the change in the land cover from primary and plantation forests to agricultural land and bare land, which increased the soil loss. According to Brodie & Catherine (2020), the vegetation canopy and ground covers can help to reduce soil erosion.
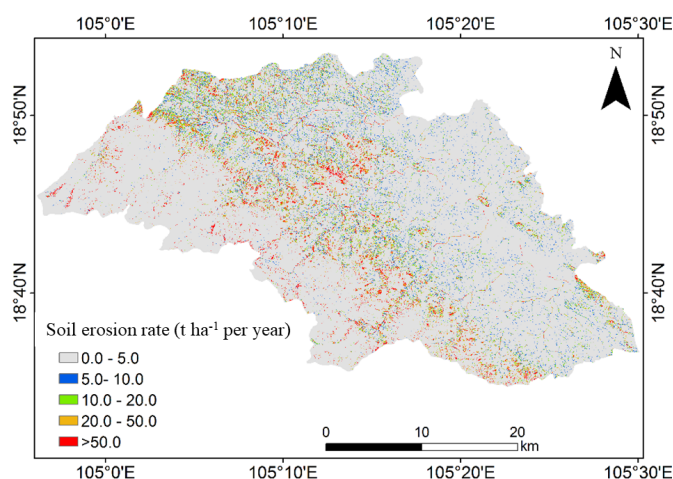
The impact of the cover factor on the soil erosion is lower because the largest components of the land cover are forest and plantation crops.

This study was conducted based on images that were acquired at different times. Due to the differences in the times at which the downloaded images were recorded, it was possible for the land coverage to experience large changes, which contributed to the C_factor and finally the soil loss in the study area.

CONCLUSIONS

1. The annual average soil loss across the Thanh Chuong Mountainous district of Nghe An province simulated by the RUSLE model is approximately 25 t per year.

2. The amount of erosion varies mainly according to the slope of topography, land cover, and rainfall intensity. The erosion severity map revealed that about 18% of the area falls under the high and very high erosion categories.

3. Overall, the high soil loss rates are related to weather conditions, the soil texture, terrain features, and unsustainable land use management practices.

ACKNOWLEDGEMENT

LITERATURE CITED

Abdo, H.; Salloum J. Mapping the soil loss in Marqya basin: Syria using RUSLE model in GIS and RS techniques. Environmental Earth Sciences v.76, p.1-10, 2017. https://doi.org/10.1007/s12665-017-6424-0

Allafta, H.; Opp, C. Soil erosion assessment using the RUSLE model, remote sensing, and GIS in the Shatt Al-Arab Basin (Iraq-Iran). Applied Sciences. v.12, p.1-17, 2022. https://doi.org/10.3390/app12157776

Amellah, O.; El-Morabiti, K. Assessment of soil erosion risk severity using GIS, remote sensing and RUSLE model in Oued Laou Basin (North Morocco). Soil Science Annual. v.72, p.1-11, 2021. https://doi.org/10.37501/soilsa/142530

Brodie, V.; Catherine, M.P. Alpine vegetation in the context of climate change: A global review of past research and future directions. Science of The Total Environment. v.748, p.1-17, 2020. https://doi.org/10.1016/j.scitotenv.2020.141344

Dang, T.A. Grain yield optimisation in the Plain of Reeds in the context of climate variability. Revista Brasileira de Engenharia Agrícola e Ambiental. v.25, p.591-596, 2021. http://dx.doi.org/10.1590/1807-1929/agriambi.v25n9p591-596

Dinh, T.K.H.; Kazuto, S.M. Effects of forest reclamation methods on soil physicochemical properties in North-Central Vietnam. Research on Crops. v.23, p.110-118, 2022. https://doi.org/10.31830/2348-7542.2022.016

Figure 5. Soil erosion map of the study area

Do, T.N. Drivers of deforestation and forest degradation in Nghe An province under the context of climate action: case study in the two communes of con cuong and Thanh Chuong districts. Master's thesis. Vietnam National University, Hanoi-Vietnam Japan University, 2020.

El-Jazouli, A.; Barakat, A.; Ghafiri, A.; El-Moutaki, S.; Ettaqy, A.; Khellouk, R. Soil erosion modeled with USLE, GIS, and remote sensing: a case study of Ikkour watershed in Middle Atlas (Morocco). Geoscience Letters. v.4, p.1-12, 2017. https://doi.org/10.1186/s40562-017-0091-6

Fachin, P.A.; Costa, Y.T.; Thomaz, E.L. Evolution of the soil chemical properties in slash-and-burn agriculture along several years of fallow. Science of The Total Environment. v.764, p.1-9, 2021. https://doi.org/10.1016/j.scitotenv.2020.142823

Ganasri, B. P.; Ramesh, H. Assessment of soil erosion by RUSLE model using remote sensing and GIS - A case study of Nethravathi Basin. Geoscience Frontiers. v.7, p.953-961, 2016. https://doi.org/10.1016/J.GSF.2015.10.007

Gitas, I.Z.; Douros, K.; Minakou, C.; Silleos, N.; Karydas, C. Multi-temporal soil erosion risk assessment. in N. Chalkidiki using a mModified USLE raster model, EARSEL. eProceedings, v.8, p.40-52, 2009. https://doi.org/10.2174/187152809787582507

Hung, T.T; Doyle, R.; Eyles, A.; Mohammed, C. Comparison of soil properties under tropical Acacia hybrid plantation and shifting cultivation land use in northern Vietnam. Southern Forests: a Journal of Forest Science. v.79, p.9-18, 2017. https://doi.org/10.2989/20702620.2016.1225185

Khwarahm, N.R.; Qader, S.; Ararat, K.; Al-Quraishi, A.M.F. Predicting and mapping land cover/land use changes in Erbil/Iraq using CA-Markov synergy model. Earth Science Informatics. v.141, p.393-406, 2021. https://doi.org/10.1007/s12145-020-00541-x

Leh, M.; Bajwa, S.; Chaubey, I. Impact of land use change on erosion risk: an integrated remote sensing, geographic information system and modeling methodology. Land Degradation and Development. v.24, p.409-421, 2013. https://doi.org/10.1002/ldr.1137

Lin, Z.Q.; Peng, S.Y. Comparison of multi-model simulations of land use and land cover change considering integrated constraints - A case study of the Fuxian Lake basin. Ecological Indicators. v.142, p.1-14, 2022. https://doi.org/10.1016/j.ecolind.2022.109254

Mohamed, E.K.; Hossam, E.S.; Khaled, M.D. Land cover/use change analysis and mapping of Borg El-Arab City, Egypt. Arabian Journal of Geosciences. v.13, p.1-13, 2020. https://doi.org/10.1007/s12517-020-06115-x

Sapkale, J.B.; Sinha, D.; Susware, N.K.; Susware, V.N. Flood hazard zone mapping of kasari river basin (Kolhapur, India), using remote sensing and GIS techniques. Journal of the Indian Society of Remote Sensing. v.50, p.2523-2541, 2022. https://doi.org/10.1007/s12524-022-01610-y

Tue, M.V.; Raghavan, S.V.; Pham, D.M.; Liong, S.Y. Investigating drought over the Central Highland, Vietnam, using regional climate models. Journal of Hydrology, v.526, p.265-273, 2015. https://doi.org/10.1016/j.jhydrol.2014.11.006

Vijith, H.; Dodge, W.D. Spatio-temporal changes in rate of soil loss and erosion vulnerability of selected region in the tropical forests of Borneo during last three decades. Earth Science Informatics, v.11, p.171-181, 2017. https://doi.org/10.1007/s12145-017-0321-7

Wischmeier, W.H.; Smith, D.D. Predicting Rainfall Erosion Losses: A Guide to Conservation Planning. Agriculture Handbook, 282. USDA-ARS, 1978.

Yesuph, A.Y.; Dagnew, A.B. Soil erosion mapping and severity analysis based on RUSLE model and local perception in the Beshillo Catchment of the Blue Nile Basin, Ethiopia. Environmental Systems Research. v.8, p.1-17, 2019. https://doi.org/10.1186/s40068-019-0145-1